Article

Large crystalline domains and enhanced exciton diffusion length enable efficient organic solar cells

Yiwei Zhang, Muhammad T. Sajjad, Oskar Blaszczyk, Andrew J. Parnell, Arvydas Ruseckas, Luis A. Serrano, Graeme Cooke, and Ifor D. W. Samuel

Chem. Mater., **Just Accepted Manuscript** • DOI: 10.1021/acs.chemmater.8b05293 • Publication Date (Web): 01 Apr 2019

Large crystalline domains and enhanced exciton diffusion length enable efficient organic solar cells

Yiwei Zhang[1‡], Muhammad T. Sajjad[1‡], Oskar Blaszczyk[1], Andrew J. Parnell[2], Arvydas Ruseckas[1], Luis A. Serrano[3], Graeme Cooke[3] and Ifor D. W. Samuel[1*]

1.Organic Semiconductor Centre, SUPA, School of Physics and Astronomy, University of St Andrews, St Andrews, KY16 9SS, UK

2. Department of Physics and Astronomy, University of Sheffield, Sheffield, S3 7RH, UK

3. Glasgow Centre for Physical Organic Chemistry, WESTCHEM, School of Chemistry, University of Glasgow, Glasgow G12 8QQ, UK

ABSTRACT: We studied crystallinity and exciton harvesting in bulk heterojunctions of the semiconducting polymer PffBT4T-2OD and electron acceptor $PC_{71}BM$ which are used to make highly efficient organic solar cells. Grazing incidence wide-angle X-ray scattering (GIWAXS) shows that the size of crystalline domains of PffBT4T-2OD increases to ~18 nm in photovoltaic blends upon thermal annealing at 100 °C for 5 minutes. These domains are larger than the typical exciton diffusion lengths in conjugated polymers. Time-resolved fluorescence measurements show that exciton diffusion length in PffBT4T-2OD increases from ~14 to ~24 nm upon thermal annealing, which enables efficient charge generation in blends with large domains. Solar cells prepared using thermally annealed blends show higher photocurrent, open circuit voltage and fill factor compared to as spin-coated blends which indicates reduced recombination losses. Our results demonstrate the advantages of large crystalline domains in organic photovoltaics, providing exciton diffusion is sufficient.

1. Introduction

Organic photovoltaics (OPVs) offer many attractive features such as simple fabrication of lightweight thin film solar cells which can be deposited on flexible substrates, low cost and short energy payback time.[1, 2] The past decade witnessed rapid development of OPVs, leading to single bulk heterojunction (BHJ) OPV devices with power conversion efficiencies (PCE) of over 12% - a value which is considered sufficient for commercialization.[3-6] However, improvements in OPV to reach 20% should be achievable [7]. To achieve higher PCE, efforts should be made in two directions.[8] Firstly, new organic semiconducting donor and acceptor materials with more favorable energy levels need to be designed and synthesized; secondly, film fabrication and post-deposition treatment methods should be optimized to rationally control the nanoscale morphology of the bulk heterojunction. Primary excitations in OPVs are bound singlet excitons which need to dissociate into free charges in order to contribute to photocurrent.[9, 10] The exciton dissociation can either realized via Förster resonance-energy transfer (FRET) or diffusion to a donor/acceptor interface. [11-14] The exciton diffusion length (L_D), defined as the distance excitons can travel within their lifetime, is a key parameter in OPV devices as it largely determines the generation of charges from excitons and thus the short circuit current and device efficiency.[15] Because the exciton diffusion length in organic semiconductors is short (typically ~10 nm), a high extent of mixing between donor and acceptor materials is desirable to obtain efficient charge separation. However, after dissociation, free charge carriers need to be extracted to the electrodes to generate current. Large donor and acceptor domains would be best for this as they reduce the interface area and associated recombination losses. Hence there is a trade-off between the desired domain size for charge generation and the size desired for charge extraction. Increasing exciton diffusion length can help to solve this problem by enabling efficient exciton harvesting from larger domains.

The exciton diffusion length of organic semiconducting materials has been measured using different techniques, including volume quenching, [16] surface quenching,[17] exciton-exciton annihilation,[18, 19] spectrally resolved photoluminescence quenching,[20] and photovoltage measurements.[21] A lot of effort has been made to enhance the exciton diffusion length by, for example, post deposition treatments such as thermal annealing, solvent vapor annealing and light soaking. Out of these, thermal annealing and solvent vapor annealing are simple, widely used and cost-efficient strategies which allow modification of the crystallinity of the film in a controllable fashion. We have previously shown that thermal annealing and solvent vapor annealing are effective to improve the exciton diffusion for some organic donor materials. [22, 23]

Recently, a highly efficient donor polymer Poly[(5,6-difluoro-2,1,3-benzothiadiazol-4,7-diyl)- alt-(3,3’’’-di(2-octyldodecyl) -2,2’ ;5’, 2’’;5’’,2’’’ -quaterthiophen-5,5’’’-diyl)], henceforth named as PffBT4T-2OD (chemical structure is shown in Figure 1(a)), has been designed and synthesized; single BHJ OPV devices using it as the donor material have achieved PCE of over 11%.[24] The processing parameters have

been shown to be crucial in determining the aggregation behavior of this polymer. [25] The structural analysis by small angle neutron scattering (SANS) showed that thermal annealing at 100 °C for 5 minutes results in coarsening of domains within the PffBT4T-2OD:$PC_{71}BM$ bulk heterojunction films from ~9 to ~13 nm, and that the OPV device efficiency was improved by 20% (from 7.6% to 8.9%). [26] Recently, because of the development of non-fullerene acceptors, solar cells with higher PCE and new physical phenomena have been reported using PffBT4T-2OD as donor material and non-fullerene acceptors. [27-32] The aim of the present work is to understand how thermal annealing increases the efficiency of the solar cells. To establish a better understanding of the exciton diffusion in the donor material, we used the well-known acceptor $PC_{71}BM$. By combining the complementary techniques of GIWAXS, time-resolved spectroscopy, space charge limited current (SCLC) and photocurrent analysis, we investigated the effect of thermal annealing on domain size, exciton diffusion length, charge mobility and charge extraction. We find that upon thermal annealing, the crystallite size increases from ~13 to ~18 nm, exciton diffusion coefficient from 0.9×10^{-3} to 2.7×10^{-3} cm^2/s and a corresponding 1-dimensional exciton diffusion length from 14.4 to 24.1 nm. Large crystallite size is beneficial for better charge extraction and long exciton diffusion length helps to realize the highly efficient exciton dissociation. The combined effect of both larger crystallite domain size and longer exciton diffusion length leads to an enhancement of more than 20% in device efficiency. This work differs from our previous work on small molecules where we used solvent vapor annealing to enhance the exciton diffusion and device performance.[33] In the present work, we use a more efficient donor polymer with the main focus on the widely used technique of thermal annealing and the use of X-ray to explore the structural changes occurring.

2. Experimental methods

Film fabrication and characterization The PffBT4T-2OD was purchased from California Organic Semiconductors Inc, it was dissolved in a solvent mixture of chlorobenzene (CB): o-dichlorobenzene (oDCB): 1,8-Diiodooctane (DIO) (volume ratio 48.5: 48.5: 3) and stirred at 90°C overnight before spin coating. The solution with polymer concentrations ranging from 3 to 14 mg/ml was spin-coated at 1000 rpm to form films of thicknesses ranging between 45 and 300 nm; the thicknesses were determined by spectroscopic ellipsometry. To investigate the effect of thermal annealing, for all the experiments, two sets of samples were prepared: one set was thermally annealed at 100 °C for 5 minutes and another set was without post deposition treatments for comparison purpose. The processing of PffBT4T-2OD films was all conducted in a nitrogen-filled glove box. For GIWAXS experiments and device fabrication, SiO_2 and glass with pre-patterned ITO substrates were used respectively; for exciton diffusion measurements, films were spin coated on fused silica substrates. All the substrates were ultrasonically cleaned in acetone, isopropanol and deionized water sequentially, each for 5 minutes; followed by oxygen plasma treatment for 3 minutes before use.

Absorbance was determined using a Cary 300 UV-visible spectrophotometer; steady state photoluminescence (PL) spectrum was recorded using an Edinburgh Instrument FLS980 Spectrometer; the excitation wavelength of 515 nm was used.

GIWAXS measurements were performed using a Xeuss 2.0 SAXS/WAXS laboratory beamline using a liquid Gallium MetalJet (Excillum) X-ray source (9.2 keV, 1.34Å); scattered X-rays were detected by a Pilatus3R 1M detector.

OPV device fabrication and characterization For OPV device fabrication, the conventional structure of ITO/PEDOT:PSS/active layer/Ca/Al was used (as shown in Figure 1(c)). PEDOT:PSS (Clevios Al 4083) was spin coated onto the pre-cleaned substrates and then annealed at 120°C for 10 minutes in the air before being transferred to the glove box. Then the blend of PffBT4T-2OD:$PC_{71}BM$ (weight ratio of 1:1.2) was spin coated from the solution of the above-mentioned solvent mixture with a total concentration of 20 mg/ml. After drying for 3 hours in a glove box and further 30 minutes in a vacuum chamber, one set of the films were annealed at 100°C for 5 minutes. Then the electrodes consisting of calcium (5 nm) and aluminum (100 nm) was evaporated in a thermal evaporator under the vacuum of $\sim 10^{-6}$ mbar. The devices were finally encapsulated using UV-cured epoxy and a glass slice.

The photovoltaic properties were characterized by a Sciencetech solar simulator and a Keithley 2400. The irradiance level was calibrated by a silicon detector and a KG-5 filter. The devices were exposed to AM1.5 solar spectrum with the irradiance level of 100 mW/cm^2 during J-V characterization. The external quantum efficiency (EQE) was measured by exposing the device to monochromatic light supplied from a Xenon arc lamp and a monochromator. The lifetime study was performed in ambient conditions under continuous illumination of the same solar simulator.

Exciton diffusion measurements For the fluorescence surface quenching measurements, a cross-linked fullerene derivative [6,6]-phenyl-C61-butyric acid styryl dendron ester (PCBSD) was used to perform as a fluorescence quencher. To prepare the quencher layer, PCBSD was dissolved in dichlorobenzene solution and stirred at 75 °C for at least 5 hours. The solution was filtered through a 0.1 μm PTFE filter before being spin coated onto a fused silica substrate. The resultant films were then annealed at 170 °C for 40 min to realize cross-linking and spinning washed by chlorobenzene to remove any un-crosslinked residuals. All the processing of cross-linked PCBSD was also conducted in a nitrogen-filled glove box. The PffBT4T-2OD films were fabricated on top of fused silica and cross-linked PCBSD respectively. Different concentration was selected to realize five sets of films with different thicknesses. Time-resolved fluorescence decay measurements were conducted under vacuum. The samples were excited by 200 fs light pulses at 515 nm and time-resolved fluorescence was recorded using a Hamamatsu streak camera.

For exciton−exciton annihilation, PffBT4T-2OD films were spin-coated on fused silica substrates; the as spin-coated and thermally annealed films were excited by 200 fs laser pulses at 650 nm and 5 kHz repetition rate with pulse energy ranging from 2 to 30 nJ and illuminated by a beam of area 0.030 mm^2. The pulses were generated using an optical parametric amplifier (OPA) pumped by a Pharos regenerative amplifier (RA) from Light Conversion Ltd. Time-resolved fluorescence was recorded using a Hamamatsu streak camera. We also measured the natural fluorescence decay in the

absence of annihilation, where pulses of lower energy (oscillator powered laser with 515 nm wavelength and 80MHz repetition rate) were used as exciting light.

3.Results

3.1 Film characterization and OPV device performance

The absorption spectra of PffBT4T-2OD: $PC_{71}BM$ blend films before and after thermal annealing are shown in Figure 1 (b). The absorption peaks at 689 nm and 627 nm can be attributed to 0-0 and 0-1 vibronic transitions of PffBT4T-2OD. The main change is a ~4% increase in the absorbance upon thermal annealing. The PL spectrum of the thermally annealed film shows a peak that is ~50% stronger at ~780 nm.

We fabricated and characterized OPV devices with and without thermal annealing treatment of the active layer. The results of the best and average of 12 devices are presented in **Figure 1 (d)** and **Table 1**. The short circuit current density (J_{sc}) was higher in the devices prepared with a thermally annealed blend (17.3 mA/cm^2 compared to 16.3 mA/cm^2 for the as spin-coated device). The results also confirmed by EQE measurements as shown in Figure S1. We also observed that V_{oc} and *FF* are higher in thermally annealed devices. The overall device efficiency was enhanced from 7.3% to 9.0% by thermal annealing.

3.2 Thermal annealing induced crystallite size growth

To understand the reason behind the improved device efficiency we investigated the crystallinity of PffBT4T-2OD:$PC_{71}BM$ BHJ films using GIWAXS and the results are shown in **Figure 2**. The Bragg peaks at q = 0.30 Å^{-1} and q = 0.59 Å^{-1} were identified as the (100) and (200) crystalline planes defined by stacking of the alkyl chains. The peak at q = 1.79 Å^{-1} corresponds to the π- π stacking distance of the polymer. These peaks become narrower upon thermal annealing which suggests to larger crystallites of PffBT4T-2OD.

The crystallite size of PfffBT4T-2OD can be obtained from the full width at half maximum (FWHM) of the (100) peak in the GIWAXS spectra using the Scherrer equation:

$$D = \frac{K\lambda}{\beta \cos\theta} \qquad (1)$$

Here K is the dimensionless shape factor, which is 0.94 in our case; λ = 0.134 nm is the X-ray wavelength used in the measurements; β is the FWHM of the peak (in radians) and θ is the Bragg angle. We found that the crystallite size of PffBT4T-2OD in the blends increases from 13.2 to 17.7 nm upon thermal annealing (see **Table 2**). We also measured the crystallite size of neat films of PffBT4T-2OD and observed enhancement from 8.8 to 15.1 nm. Our results are consistent with the previous reports where the coarsening of PffBT4T-2OD domains in the bend with $PC_{71}BM$ was observed.[26]

3.3 Effect of thermal annealing on exciton diffusion

We used two methods to measure exciton diffusion in PffBT4T-2OD: surface quenching of fluorescence and exciton-exciton annihilation. For the first method, the fluorescence decays were measured in films deposited on the cross-linked fullerene derivative and compared with decays measured on a non-quenching fused silica substrate. These measurements were performed at low excitation density where exciton-exciton annihilations can be neglected. In that case, the dynamics of exciton density N can be described by the diffusion equation: [34, 35]

$$\frac{\partial N}{\partial t} = D\frac{\partial^2 N}{\partial x^2} - kN - k_F N + G(x) \qquad (2)$$

where k_F is quenching rate due to Förster resonance energy transfer (FRET) to the quencher, $G(x)$ is the exciton generation rate as a function of position, D is exciton diffusion coefficient and k is the natural decay rate of excitons.

To obtain the diffusion coefficient, we made several assumptions to solve the diffusion equation: exciton generation is instantaneous as our excitation light pulse is short. No FRET is considered as there is no spectral overlap due to the absorption of PCBSD being at a much shorter wavelength than the emission of PffBT4T-2OD.[36] We assume no quenching occurs at the top surface, which gave the boundary condition of $\partial N/\partial x = 0$ at $x=d$, where d is the thickness of the polymer film. At the PffBT4T-2OD/ PCBSD interface, we assume all excitons are quenched giving the second boundary condition of $N = 0$ at $x=0$.

The diffusion equation can be solved numerically. We obtain the exciton diffusion coefficient (D) by performing a globe fit to all the fluorescence decays of the PffBT4T-2OD films on top of PCBSD. In this procedure, D is the only fitting parameter. The experimental and fitted results for the five sets of samples are illustrated in **Figure 3**. The results show that the average diffusion coefficient increased from 0.8 × 10^{-3} to 2.4 × 10^{-3} cm^2/s upon thermal annealing.

The surface quenching method measures exciton diffusion in the direction perpendicular to the film surface, however, in BHJ the shortest distance to the electron acceptor could be in any direction. To characterize exciton diffusion in the bulk of the film we used exciton-exciton annihilation measurements (detail given in SI) by measuring time-resolved PL as a function of initial excitation density (Figure 4). Figure 4 (a) and (b) show that fluorescence decays became faster with higher initial exciton populations due to exciton-exciton annihilation.

We fitted the fluorescence decays using Equation (S2) to obtain the annihilation rate constant γ(t) which is shown in Figure 4 (c). It can be seen that annihilation rate constant increased significantly after thermal annealing. The exciton diffusion coefficients determined from the annihilation rate constant are 1.0 × 10^{-3} and 3.0 × 10^{-3} cm^2/s for as spin-coated and thermally annealed films respectively. We used a value of 2.1 nm for the annihilation radius R_a which is the d_{100} spacing value determined from X-ray data. These values of D are similar to the values obtained using surface quenching which imply that exciton diffusion is isotropic in PffBT4T-2OD. More discussion can be found in SI. We calculated the 1-dimensional and 3-dimensional exciton diffusion length i. e. $L_D = \sqrt{2D\tau}$ and $L_{3D} = \sqrt{6D\tau}$ using the lifetime value determined from the fluorescence decay in absence of annihilation (values are indicated in Figure 4).

We summarize the exciton diffusion results obtained from the two different methods in **Table 3**. It can be seen, from both measurements, the exciton diffusion coefficient

increased by a factor of 3 upon thermal annealing. As the lifetime did not show a significant decrease (being ~1160 and ~1090 ps for as spin-coated and thermally annealed films respectively), the corresponding 1-dimensional exciton diffusion length increased from ~14 nm to ~24 nm and 3-dimensional exciton diffusion length from ~ 25 nm to ~ 42 nm.

3.4 PffBT4T-2OD domain size determined by PL quenching

We performed an additional measurement of the domain size of the donor by measuring the time-resolved PL of the PffBT4T-2OD:$PC_{71}BM$ blends. The results are shown in Figure 5 which also shows the PL decays of pure PffBT4T-2OD with and without thermal annealing. Compared to pure films, blends show faster PL decay due to exciton dissociation at the interface between donor and acceptor. Among the blends, thermally annealed shows slower decay indication larger crystallite size (domains).

We extracted the size of the PffBT4T-2OD domains in the blend using an approach similar to Hedley et al[37] and Jagadamma et al[38] by considering that PL quenching of the donor in the blend is mediated by exciton diffusion. We assume that the exciton diffuses inside the sphere of the donor (which is surrounded by a $PC_{71}BM$ matrix) by a random walk and is then quenched at the surface of the sphere. Then the number of excitons $N(t)$ on donor molecules is expected to decay with time as follows

$$N(t) = \frac{6}{\pi^2}\sum_{m=1}^{\infty}\frac{1}{m^2}\exp\left(\frac{D\pi^2 m^2 t}{r^2}\right) \qquad (3)$$

where D is the exciton diffusion coefficient and r is the radius of the sphere. We used the experimentally measured D = 1.0 × 10^{-3} cm^2/s for unannealed film and D = 3.0 × 10^{-3} cm^2/s for thermally annealed film.

For fitting, we multiplied equation 2 with the fluorescence intensity of pure PffBT4T-2OD film and then used it to fit the PL decay of the blends (shown in Figure 5). The time-resolved PL measurements suggest that the domain size of PffBT4T-2OD increases from ~12 nm to ~29 nm upon thermal annealing. The general trend of a larger domain size after thermal annealing is the same as for X-ray, but the results differ quantitatively. This could be because of some of the assumptions made in the analysis of the PL such as assuming the donor is spherical in shape, and assuming donor and acceptor phases are entirely separate.

3.5 Charge transport, extraction and recombination

To investigate charge transport, we fabricated hole only devices with the structure of ITO/PEDOT:PSS/PffBT4T-2OD:$PC_{71}BM$/MoO_3/Ag to characterize the hole mobility using SCLC theory [39]. We found a hole mobility of 6.5 × 10^{-4} V^{-1} s^{-1} for as-spin coated and 1.9 × 10^{-3} cm^2 V^{-1} s^{-1} for thermally annealed films (See **Figure 6(a)**) The results show that the higher crystallinity and larger domain size do indeed result in higher hole mobility which in turn favors better charge transport.

Information about charge extraction can be determined from the relationship between photo-generated current (J_{ph}) and effective voltage (V_{eff}), with J_{ph} defined as the difference between current density under illumination (J_L) and current density in the dark (J_D); and V_{eff} is defined as $V_{BI} - V_{app}$ where V_{BI} is the voltage when J_{ph} = 0 and V_{app} is applied bias voltage.[40, 41] The results have been shown in Figure 6(b), the photocurrent increased linearly with voltage at low V_{eff}, and saturated at high V_{eff} indicating all of the charges are driven to electrodes. The charge collection probability (P_c), defined as J_{ph} / $J_{ph,sat}$, can be used to evaluate the fraction of charges extracted from the solar cell. As shown in Figure 6(c), the charge collection probability at short circuit condition (V_{eff} = V_{BI}) of as spin-coated and thermally annealed devices were 91.6% and 95.6% respectively. These results suggest that the charge extraction was more efficient in the thermally annealed devices compared to the as spin-coated devices.

To explore the charge recombination mechanism, we investigated the dependence of V_{oc} on light intensity.[42] At open circuit, no current is generated, and all charges recombine. A plot of V_{oc} against log (light intensity) is in Figure 6(d). If bimolecular recombination dominates, the slope should be almost equal to k_BT/q, where k_B is the Boltzmann constant, T is temperature and q is elementary charge. A slope steeper than k_BT/q suggests the existence of trap-assisted charge recombination. [43] It can be seen from Figure 6(d) that the slope of as spin-coated devices (1.60 k_BT/q) was larger than that of thermally annealed devices (1.34 k_BT/q). This indicates less trap-assisted recombination occurs in thermally annealed devices, which is consistent with their better device performance observed.

3.6 Effect of thermal annealing on stability of solar cells

Our encouraging results on the effects of thermal annealing on device performance mean that it is also desirable to explore its effect on device lifetime. It is known that devices based on PffBT4T-2OD and fullerene acceptors suffer from a large burn-in loss. [44] This is due to the spinodal demixing of fullerene acceptor and the donor polymer and has been explained in terms of the interaction parameter (χ) of this polymer-fullerene combination.[45] Replacing the fullerene acceptor with non-fullerene acceptors can solve this problem and largely enhance the stability of PffBT4T-2OD based solar cells. [46] The issue we investigate here is whether thermal annealing of our fullerene containing devices improves or worsens their lifetime. We therefore tested the stability of as spin-coated and thermally annealed devices following the testing protocol of ISOS-L-1, [47, 48] (i.e. under constant illumination of AM1.5 solar spectrum with intensity of 100 mW/cm^2 in ambient atmosphere). As shown in Figure S3, the device efficiency dropped rapidly in the first hour for both as spin-coated and thermally annealed devices. The fast degradation was primarily due to a rapid drop of J_{sc}, with V_{oc} and FF decreasing at a slower rate. The rapid decrease of J_{sc} is a result of the use of a chlorinated solvent. PffBT4T-2OD solar cells using a non-fullerene acceptor fabricated from mesitylene solution are reported to have better stability than devices deposited from chlorobenzene solution. [49] The decrease in efficiency with time is much smaller for thermally annealed devices than for as spin-coated ones. After 5 hours continuous light exposure, the efficiency dropped to ~20% of its original value for thermally annealed devices; while the as spin-coated devices only retained ~5% of their original efficiency. Cha et al. [46] found that solar cells using PffBT4T-2OD: $PC_{71}BM$ active layer degraded very rapidly under 85°C thermal stress in an inert atmosphere, due to thermally induced phase segregation. However, in our study, the thermally annealed devices have better stability. These results are not

contradictory, as we annealed the devices for 5 minutes, rather than applying constant thermal stress. It has been proved employing DIO can enhance the initial device efficiency by optimizing the BHJ morphology, but significantly increase the efficiency loss during burn-in period.[50, 51] A possible reason for our observation of better stability in thermally annealed devices is that thermal annealing removes DIO completely from the BHJ films. It has been shown that DIO remains in the film after vacuum electrode deposition, [51] but thermal annealing at 100 °C for 5 minutes can remove it completely.[26]

4. Discussion

We begin by considering the higher steady state PL intensity in thermally annealed PffBT4T-2OD: $PC_{71}BM$ blend films compared to the as spin-coated counterpart. This is due to reduced quenching by the acceptor. It is consistent with the slower decay of the time-resolved PL of the thermally annealed films (Figure 5) and the larger domain size inferred from it.

We next consider why the exciton diffusion length increases in the thermally annealed films. It has been shown by simulation and experiments that exciton diffusion coefficient is highly dependent on the crystallinity of the film. In highly crystalline regions, exciton diffusion coefficient is much higher than in amorphous regions. [52, 53] In our case, thermal annealing increased the crystallite size, thus reducing the amount of amorphous materials; and so increasing the exciton diffusion coefficient.

Finally, we discuss the better OPV device performance in thermally annealed films and investigate what factors influence this enhancement. From X-ray, we find that the crystallite size increases by 40% upon thermal annealing (i.e. from 13 nm to 18 nm). The larger crystal domain size is usually favourable for higher V_{oc} and *FF* as there is less recombination. This is supported by the V_{oc} measurements at various light intensity in Figure 6(d). In addition, charge transport and extraction are also determined to be more efficient with bigger domain sizes leading to an improvement in J_{sc}. However, with the crystallite domain size exceeding the typical exciton diffusion length of most conjugated polymers, exciton dissociation might be expected to be less efficient, giving lower J_{sc}. However, as Figure 1(d) shows this is not observed. The high short circuit current is maintained in spite of large domains. this is because the thermal annealing increased the exciton diffusion length to be similar to the crystallite size. The enhanced exciton diffusion length enables efficient exciton dissociation; whilst the larger domains facilitate charge extraction and reduce charge recombination, leading to improved device performance.

5. Conclusion

In conclusion, we investigated the effect of thermal annealing on crystallite size, exciton diffusion and charge harvesting in PffBT4T-2OD:$PC_{71}BM$ BHJ solar cells. It was found that thermal annealing can significantly increase the crystallite size of PffBT4T-2OD to be bigger than the typical exciton diffusion length for conjugated polymers. However, as the exciton diffusion length was also increased from ~14 to ~24 nm, exciton harvesting is still efficient even in thermally annealed films with large donor crystallite size. The large domains improve the charge extraction efficiency and reduce the charge recombination problem in the devices. Hence our results show that thermal annealing increases both domain size and exciton diffusion length which then lead to an enhancement in the device performance.

ASSOCIATED CONTENT

Supporting Information including: EQE measurements of solar cells, details of exciton-exciton annihilation measurements, hole mobility measured by SCLC method, operational stability of solar cells, is available free of charge via the Internet at http://pubs.acs.org. The data supporting this work can be accessed through: https://doi.org/10.17630/6fb583c8-92b9-45ab-9040-de8ee764c517

AUTHOR INFORMATION

Corresponding Author

* Ifor D. W. Samuel email: idws@st-andrews.ac.uk

Author Contributions

‡These authors contributed equally.

Notes

The authors declare no competing financial interest.

ACKNOWLEDGMENT

We thank the European Research Council for financial support (EXCITON grant 321305) and Dr. L. K. Jagadamma for helpful discussions.

REFERENCES

1. Dou, L.; You, J.; Hong, Z.; Xu, Z.; Li, G.; Street, R. A.; Yang, Y., 25th Anniversary Article: A Decade of Organic/Polymeric Photovoltaic Research. *Adv. Mater.* **2013,** 25, (46), 6642-6671.

2. Brabec, C. J.; Gowrisanker, S.; Halls, J. J. M.; Laird, D.; Jia, S. J.; Williams, S. P., Polymer-Fullerene Bulk-Heterojunction Solar Cells. *Adv. Mater.* **2010,** 22, (34), 3839-3856.

3. Yanbo, W.; Yamin, Z.; Nailiang, Q.; Huanran, F.; Huanhuan, G.; Bin, K.; Yanfeng, M.; Chenxi, L.; Xiangjian, W.; Yongsheng, C., A Halogenation Strategy for over 12% Efficiency Nonfullerene Organic Solar Cells. *Adv. Energy Mater.* **2018,** 8, 1702870.

4. Cheng, P.; Li, G.; Zhan, X.; Yang, Y., Next-generation organic photovoltaics based on non-fullerene acceptors. *Nat. Photonics* **2018,** 12, (3), 131-142.

5. Li, S.; Ye, L.; Zhao, W.; Zhang, S.; Mukherjee, S.; Ade, H.; Hou, J., Energy□Level Modulation of Small□Molecule Electron Acceptors to Achieve over 12% Efficiency in Polymer Solar Cells. *Adv. Mater.* **2016,** 28, (42), 9423-9429.

6. Wenchao, Z.; Sunsun, L.; Shaoqing, Z.; Xiaoyu, L.; Jianhui, H., Ternary Polymer Solar Cells based on Two Acceptors and One Donor for Achieving 12.2% Efficiency. *Adv. Mater.* **2017,** 29, (2), 1604059.

7. Kirchartz, T.; Taretto, K.; Rau, U., Efficiency Limits of Organic Bulk Heterojunction Solar Cells. *J. Phys. Chem. C* **2009,** 113, (41), 17958-17966.

8. Green, M. A.; Bremner, S. P., Energy conversion approaches and materials for high-efficiency photovoltaics. *Nat. Mater.* **2016,** 16, 23.

9. Li, G.; Zhu, R.; Yang, Y., Polymer solar cells. *Nat. Photonics* **2012,** 6, (3), 153-161.
10. Blom, P. W.; Mihailetchi, V. D.; Koster, L. J. A.; Markov, D. E., Device physics of polymer: fullerene bulk heterojunction solar cells. *Adv. Mater.* **2007,** 19, (12), 1551-1566.
11. Barford, W.; Tozer, O. R., Theory of exciton transfer and diffusion in conjugated polymers. *J. Chem. Phys.* **2014,** 141, (16), 164103.
12. Ward, A. J.; Ruseckas, A.; Samuel, I. D., A Shift from Diffusion Assisted to Energy Transfer Controlled Fluorescence Quenching in Polymer–Fullerene Photovoltaic Blends. *J. Phys. Chem. C* **2012,** 116, (45), 23931-23937.
13. Hedley, G. J.; Ruseckas, A.; Samuel, I. D., Light harvesting for organic photovoltaics. *Chem. Rev.* **2016,** 117, (2), 796-837.
14. Sajjad, M. T.; Ward, A. J.; Ruseckas, A.; Bansal, A. K.; Allard, S.; Scherf, U.; Samuel, I. D., Tuning the Exciton Diffusion Coefficient of Polyfluorene Based Semiconducting Polymers. *physica status solidi (RRL)–Rapid Research Letters*, **2019,** 13, (3), 1800500.
15. Mikhnenko, O. V.; Blom, P. W. M.; Nguyen, T.-Q., Exciton diffusion in organic semiconductors. *Energy & Environmental Science* **2015,** 8, (7), 1867-1888.
16. Markov, D. E.; Blom, P. W. M., Anisotropy of exciton migration in poly(***p***-phenylene vinylene). *Phys. Rev. B* **2006,** 74, (8), 085206.
17. Shaw Paul, E.; Ruseckas, A.; Samuel Ifor, D. W., Exciton Diffusion Measurements in Poly(3-hexylthiophene). *Adv. Mater.* **2008,** 20, (18), 3516-3520.
18. Stevens, M. A.; Silva, C.; Russell, D. M.; Friend, R. H., Exciton dissociation mechanisms in the polymeric semiconductors poly(9,9-dioctylfluorene) and poly(9,9-dioctylfluorene-co-benzothiadiazole). *Phys. Rev. B* **2001,** 63, (16), 165213.
19. Lewis, A. J.; Ruseckas, A.; Gaudin, O. P. M.; Webster, G. R.; Burn, P. L.; Samuel, I. D. W., Singlet exciton diffusion in MEH-PPV films studied by exciton–exciton annihilation. *Org. Electron.* **2006,** 7, (6), 452-456.
20. Lunt, R. R.; Giebink, N. C.; Belak, A. A.; Benziger, J. B.; Forrest, S. R., Exciton diffusion lengths of organic semiconductor thin films measured by spectrally resolved photoluminescence quenching. *J. Appl. Phys.* **2009,** 105, (5), 053711.
21. Mullenbach, T. K.; Curtin, I. J.; Zhang, T.; Holmes, R. J., Probing dark exciton diffusion using photovoltage. *Nat. commun.* **2017,** 8, 14215.
22. Sajjad, M. T.; Ward, A. J.; Kästner, C.; Ruseckas, A.; Hoppe, H.; Samuel, I. D. W., Controlling Exciton Diffusion and Fullerene Distribution in Photovoltaic Blends by Side Chain Modification. *J. Phys. Chem. Lett.* **2015,** 6, (15), 3054-3060.
23. Long, Y.; Hedley, G. J.; Ruseckas, A.; Chowdhury, M.; Roland, T.; Serrano, L. A.; Cooke, G.; Samuel, I. D. W., Effect of Annealing on Exciton Diffusion in a High Performance Small Molecule Organic Photovoltaic Material. *ACS Applied Materials & Interfaces* **2017,** 9, (17), 14945-14952.
24. Liu, Y.; Zhao, J.; Li, Z.; Mu, C.; Ma, W.; Hu, H.; Jiang, K.; Lin, H.; Ade, H.; Yan, H., Aggregation and morphology control enables multiple cases of high-efficiency polymer solar cells. *Nat. Commun.* **2014,** 5.
25. Ma, W.; Yang, G.; Jiang, K.; Carpenter, J. H.; Wu, Y.; Meng, X.; McAfee, T.; Zhao, J.; Zhu, C.; Wang, C.; Ade, H.; Yan, H., Influence of Processing Parameters and Molecular Weight on the Morphology and Properties of High-Performance PffBT4T-2OD:PC71BM Organic Solar Cells. *Adv. Energy Mater.* **2015,** 5, (23), n/a-n/a.
26. Zhang, Y.; Parnell, A. J.; Pontecchiani, F.; Cooper, J. F. K.; Thompson, R. L.; Jones, R. A. L.; King, S. M.; Lidzey, D. G.; Bernardo, G., Understanding and controlling morphology evolution via DIO plasticization in PffBT4T-2OD/PC71BM devices. *Sci. Rep.* **2017,** 7, 44269.
27. Cha, H.; Wheeler, S.; Holliday, S.; Dimitrov, S. D.; Wadsworth, A.; Lee, H. H.; Baran, D.; McCulloch, I.; Durrant, J. R., Influence of Blend Morphology and Energetics on Charge Separation and Recombination Dynamics in Organic Solar Cells Incorporating a Nonfullerene Acceptor. *Adv. Func.l Mater.* **2018,** 28, (3), 1704389.
28. Ye, L.; Li, S.; Liu, X.; Zhang, S.; Ghasemi, M.; Xiong, Y.; Hou, J.; Ade, H., Quenching to the Percolation Threshold in Organic Solar Cells. *Joule* **2018**, 3, 443-458.
29. Baran, D.; Kirchartz, T.; Wheeler, S.; Dimitrov, S.; Abdelsamie, M.; Gorman, J.; Ashraf, R. S.; Holliday, S.; Wadsworth, A.; Gasparini, N.; Kaienburg, P.; Yan, H.; Amassian, A.; Brabec, C. J.; Durrant, J. R.; McCulloch, I., Reduced voltage losses yield 10% efficient fullerene free organic solar cells with >1 V open circuit voltages. *Energy & Environmental Science* **2016,** 9, (12), 3783-3793.
30. Wadsworth, A.; Moser, M.; Marks, A.; Little, M. S.; Gasparini, N.; Brabec, C. J.; Baran, D.; McCulloch, I., Critical review of the molecular design progress in non-fullerene electron acceptors towards commercially viable organic solar cells. *Chem. Soc. Rev.* **2019,** 48, 1596-1625.
31. Gasparini, N.; Wadsworth, A.; Moser, M.; Baran, D.; McCulloch, I.; Brabec, C. J., The Physics of Small Molecule Acceptors for Efficient and Stable Bulk Heterojunction Solar Cells. *Adv. Energy Mater.* **2018,** 8, (12), 1703298.
32. Yan, C.; Barlow, S.; Wang, Z.; Yan, H.; Jen, A. K. Y.; Marder, S. R.; Zhan, X., Non-fullerene acceptors for organic solar cells. *Nat. Rev. Mater.* **2018,** 3, 18003.
33. Sajjad, M. T.; Blaszczyk, O.; Jagadamma, L. K.; Roland, T. J.; Chowdhury, M.; Ruseckas, A.; Samuel, I. D., Engineered exciton diffusion length enhances device efficiency in small molecule photovoltaics. *J. Mater. Chem. A* **2018,** 6, (20), 9445-9450.
34. Scully, S. R.; McGehee, M. D., Effects of optical interference and energy transfer on exciton diffusion length measurements in organic semiconductors. *J. Appl. Phys.* **2006,** 100, (3), 034907.
35. Ward, A. J.; Ruseckas, A.; Samuel, I. D. W., A Shift from Diffusion Assisted to Energy Transfer Controlled Fluorescence Quenching in Polymer–Fullerene Photovoltaic Blends. *J. Phys. Chem. C* **2012,** 116, (45), 23931-23937.
36. Hsieh, C.-H.; Cheng, Y.-J.; Li, P.-J.; Chen, C.-H.; Dubosc, M.; Liang, R.-M.; Hsu, C.-S., Highly Efficient and Stable Inverted Polymer Solar Cells Integrated with a Cross-Linked Fullerene Material as an Interlayer. *J. Am. Chem. Soc.* **2010,** 132, (13), 4887-4893.
37. Hedley, G. J.; Ward, A. J.; Alekseev, A.; Howells, C. T.; Martins, E. R.; Serrano, L. A.; Cooke, G.; Ruseckas, A.; Samuel, I. D., Determining the optimum morphology in high-performance polymer-fullerene organic photovoltaic cells. *Nat. commun.* **2013,** 4.

38. Jagadamma, L. K.; Sajjad, M. T.; Savikhin, V.; Toney, M. F.; Samuel, I. D., Correlating photovoltaic properties of a PTB7-Th: PC 71 BM blend to photophysics and microstructure as a function of thermal annealing. *J. Mater. Chem. A* **2017,** 5, (28), 14646-14657.
39. Murgatroyd, P. N., Theory of space-charge-limited current enhanced by Frenkel effect. *J. phys. D: Applied Physics* **1970,** 3, (2), 151.
40. Cowan, S. R.; Street, R. A.; Cho, S.; Heeger, A. J., Transient photoconductivity in polymer bulk heterojunction solar cells: Competition between sweep-out and recombination. *Phys. Rev. B* **2011,** 83, (3), 035205.
41. Mandoc, M. M.; Veurman, W.; Koster, L. J. A.; de Boer, B.; Blom, P. W. M., Origin of the Reduced Fill Factor and Photocurrent in MDMO-PPV:PCNEPV All-Polymer Solar Cells. *Adv. Func. Mater.* **2007,** 17, (13), 2167-2173.
42. Baran, D.; Gasparini, N.; Wadsworth, A.; Tan, C. H.; Wehbe, N.; Song, X.; Hamid, Z.; Zhang, W.; Neophytou, M.; Kirchartz, T.; Brabec, C. J.; Durrant, J. R.; McCulloch, I., Robust nonfullerene solar cells approaching unity external quantum efficiency enabled by suppression of geminate recombination. *Nat. Commun.* **2018,** 9, (1), 2059.
43. Cowan, S. R.; Roy, A.; Heeger, A. J., Recombination in polymer-fullerene bulk heterojunction solar cells. *Phys. Rev. B* **2010,** 82, (24), 245207.
44. Li, N.; Perea, J. D.; Kassar, T.; Richter, M.; Heumueller, T.; Matt, G. J.; Hou, Y.; Güldal, N. S.; Chen, H.; Chen, S.; Langner, S.; Berlinghof, M.; Unruh, T.; Brabec, C. J., Abnormal strong burn-in degradation of highly efficient polymer solar cells caused by spinodal donor-acceptor demixing. *Nat. Commun.* **2017,** 8, 14541.
45. Perea, J. D.; Langner, S.; Salvador, M.; Sanchez-Lengeling, B.; Li, N.; Zhang, C.; Jarvas, G.; Kontos, J.; Dallos, A.; Aspuru-Guzik, A.; Brabec, C. J., Introducing a New Potential Figure of Merit for Evaluating Microstructure Stability in Photovoltaic Polymer-Fullerene Blends. *J. Phys. Chem. C* **2017,** 121, (33), 18153-18161.
46. Cha, H.; Wu, J.; Wadsworth, A.; Nagitta, J.; Limbu, S.; Pont, S.; Li, Z.; Searle, J.; Wyatt, M. F.; Baran, D.; Kim, J.-S.; McCulloch, I.; Durrant, J. R., An Efficient, "Burn in" Free Organic Solar Cell Employing a Nonfullerene Electron Acceptor. *Adv. Mater.* **2017,** 29, (33), 1701156.
47. Reese, M. O.; Gevorgyan, S. A.; Jørgensen, M.; Bundgaard, E.; Kurtz, S. R.; Ginley, D. S.; Olson, D. C.; Lloyd, M. T.; Morvillo, P.; Katz, E. A.; Elschner, A.; Haillant, O.; Currier, T. R.; Shrotriya, V.; Hermenau, M.; Riede, M.; R. Kirov, K.; Trimmel, G.; Rath, T.; Inganäs, O.; Zhang, F.; Andersson, M.; Tvingstedt, K.; Lira-Cantu, M.; Laird, D.; McGuiness, C.; Gowrisanker, S.; Pannone, M.; Xiao, M.; Hauch, J.; Steim, R.; DeLongchamp, D. M.; Rösch, R.; Hoppe, H.; Espinosa, N.; Urbina, A.; Yaman-Uzunoglu, G.; Bonekamp, J.-B.; van Breemen, A. J. J. M.; Girotto, C.; Voroshazi, E.; Krebs, F. C., Consensus stability testing protocols for organic photovoltaic materials and devices. *Sol. Energy Mater. Sol. Cells* **2011,** 95, (5), 1253-1267.
48. Zhang, Y.; Samuel, I. D. W.; Wang, T.; Lidzey, D. G., Current Status of Outdoor Lifetime Testing of Organic Photovoltaics. *Adv. Sci.* **2018,** 5, (8), 1800434.
49. Wadsworth, A.; Ashraf, R. S.; Abdelsamie, M.; Pont, S.; Little, M.; Moser, M.; Hamid, Z.; Neophytou, M.; Zhang, W.; Amassian, A.; Durrant, J. R.; Baran, D.; McCulloch, I., Highly Efficient and Reproducible Nonfullerene Solar Cells from Hydrocarbon Solvents. *ACS Energy Letters* **2017,** 2, (7), 1494-1500.
50. Pearson, A. J.; Hopkinson, P. E.; Couderc, E.; Domanski, K.; Abdi-Jalebi, M.; Greenham, N. C., Critical light instability in CB/DIO processed PBDTTT-EFT:PC71BM organic photovoltaic devices. *Org. Electron.* **2016,** 30, 225-236.
51. Kim, W.; Kim, J. K.; Kim, E.; Ahn, T. K.; Wang, D. H.; Park, J. H., Conflicted Effects of a Solvent Additive on PTB7:PC71BM Bulk Heterojunction Solar Cells. *J. Phys. Chem. C* **2015,** 119, (11), 5954-5961.
52. Chowdhury, M.; Sajjad, M. T.; Savikhin, V.; Hergué, N.; Sutija, K. B.; Oosterhout, S. D.; Toney, M. F.; Dubois, P.; Ruseckas, A.; Samuel, I. D. W., Tuning crystalline ordering by annealing and additives to study its effect on exciton diffusion in a polyalkylthiophene copolymer. *Phys. Chem. Chem. Phys.* **2017,** 19, (19), 12441-12451.
53. Bjorgaard, J. A.; Köse, M. E., Simulations of Exciton Diffusion and Trapping in Semicrystalline Morphologies of Poly(3-hexylthiophene). *J. Phys. Chem. C* **2014,** 118, (11), 5756-5761.

Table 1. Device metrics with and without thermal annealing.

Device type	*PCE* (%)	V_{oc} (V)	*FF* (%)	J_{sc} (mA/cm^2)
Neat	7.4 (7.3 ± 0.14) *	0.70 (0.70 ± 0.00)	65.1 (63.9 ± 1.0)	16.4 (16.3 ± 0.12)
Thermally annealed	9.2 (9.0 ± 0.19)	0.75 (0.74 ± 0.01)	72.4 (70.1 ± 1.5)	17.5 (17.3 ± 0.10)

*The value in the brackets are the average and standard deviation of 12 devices.

Table 2. Determination of PffBT4T-2OD crystallite size.

Samples	(100) peak position (2θ) (degree)	FWHM of (100) peak (radians)	Crystallite size (nm)
Pure PffBT4T-2OD (As-spin coated)	3.6523	0.01437	8.8
Pure PffBT4T-2OD (Thermally annealed)	3.6526	0.00838	15.1
PffBT4T-2OD:$PC_{71}BM$ (As-spin coated)	3.6421	0.00958	13.2
PffBT4T-2OD:$PC_{71}BM$ (Thermally annealed)	3.6147	0.00712	17.8

Table 3. Exciton diffusion properties determined by two different methods.

Methods	Surface quenching D(10^{-3}cm^2/s)	Exciton-Exciton annihilation D(10^{-3}cm^2/s)	L_{1D} (nm)	L_{3D} (nm)
As spin coated film	0.8	1.0	14.4	24.9
Thermally annealed film	2.4	3.0	24.1	41.7

*L_D is calculated according to $L_D = \sqrt{2D\tau}$ and $L_{3D} = \sqrt{6D\tau}$, τ is the time for the fluorescence decay to 1/e of its initial value in absence of annihilation.

Figure captions

Figure 1: (a) Chemical structure of PffBT4T-2OD (b) absorption coefficient and steady state photoluminescence spectra of as spin-coated and thermally annealed PffBT4T-2OD: $PC_{71}BM$ blend films. For PL measurement, films were excited at 515 nm. (c) device structure and (d) J-V curves of PffBT4T-2OD:$PC_{71}BM$ bulk heterojunction OPV devices with/without thermal annealing.

Figure 2: GIWAXS profiles for as-spin coated and thermally annealed PffBT4T-2OD: $PC_{71}BM$ blends (top) neat PffBT4T-2OD films (bottom). The GIWAXS data has been normalized to the (100) peak of PffBT4T-2OD at q=0.30 $Å^{-1}$. The graphs on the right show an expanded view of the (100) diffraction peaks.

Figure 3: Photoluminescence decays for three sets of PffBT4T-2OD films on fused silica and PCBSD substrates. (excitation wavelength was 515 nm) Fits to the data with the diffusion equation are represented by solid lines.

Figure 4: Time-resolved photoluminescence in (a) as-spin coated and (b) thermally annealed films with different initial exciton populations. (c) Annihilation rate constant (γ) in the as-spin coated and thermally annealed films extracted by fitting the time-resolved PL data with equation S2.

Figure 5: Time-resolved PL quenching of as spin-coated PffBT4T-2OD: $PC_{71}BM$ blend before and after thermal annealing and PL decay of neat PffBT4T-2OD films. TA denotes thermally annealed. Solid red lines are fits to the data using Equation 3.

Figure 6: (a) Dark J-V curves of the hole only devices. (b) Photo-generated current density as a function of effective voltage. (c) Charge collection probability as a function of effective voltage. (d) V_{oc} of devices as a function of light intensity, together with linear fits to the data.

TOC

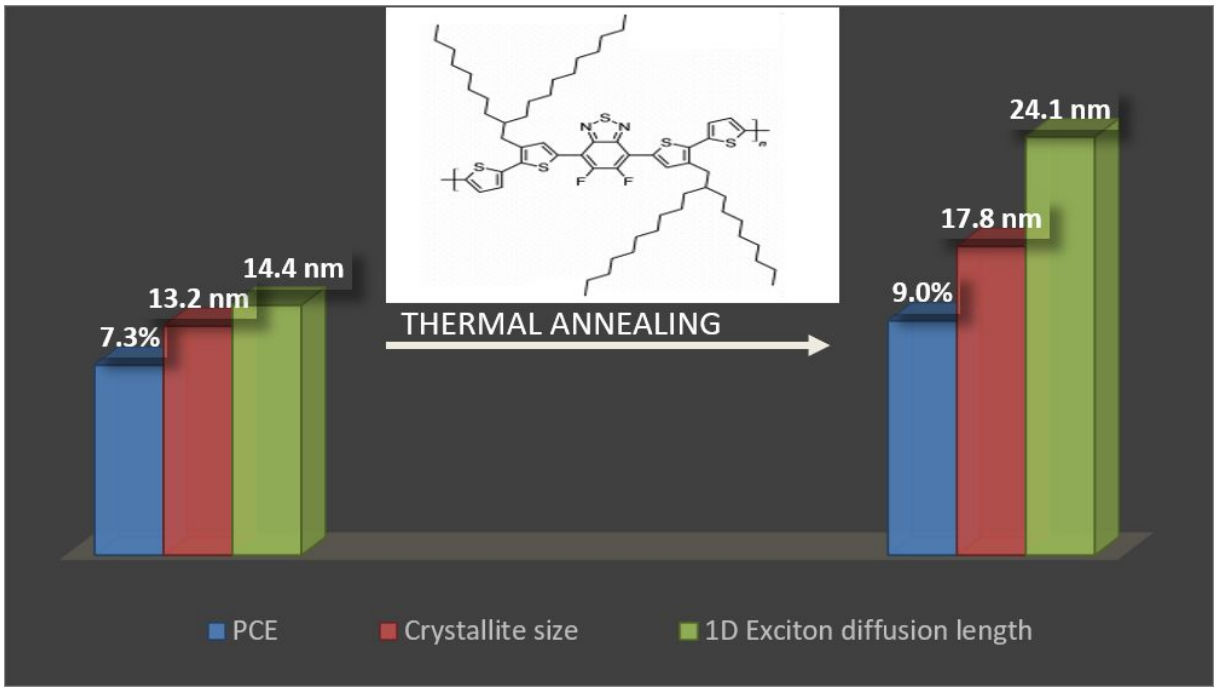
7.3%
13.2 nm
14.4 nm
THERMAL ANNEALING
9.0%
17.8 nm
24.1 nm
PCE
Crystallite size
1D Exciton diffusion length

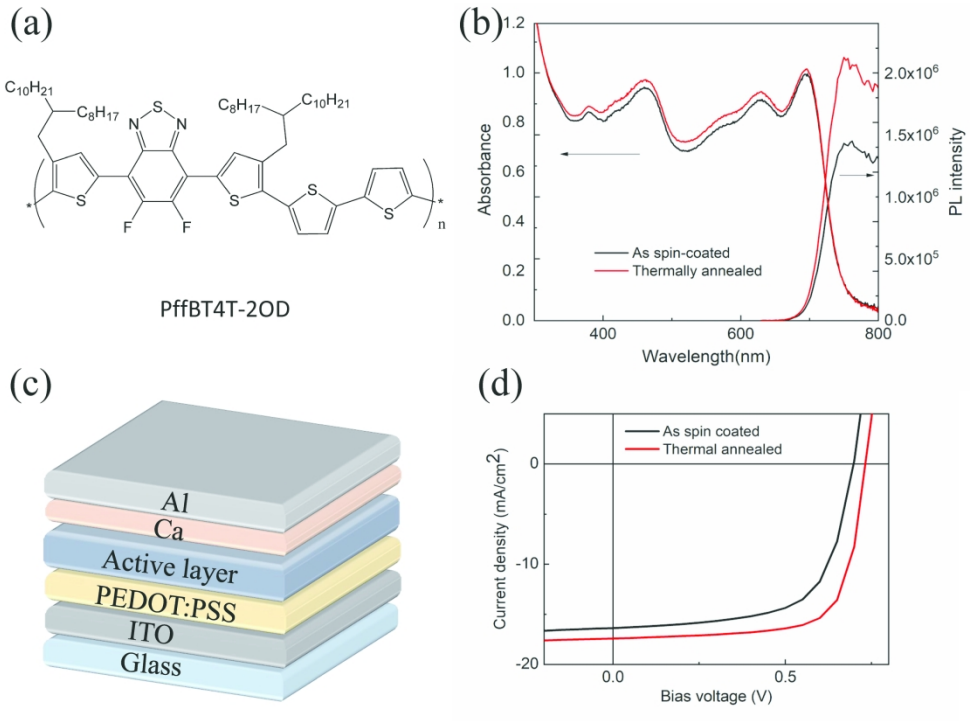

Figure 1

254x190mm (300 x 300 DPI)

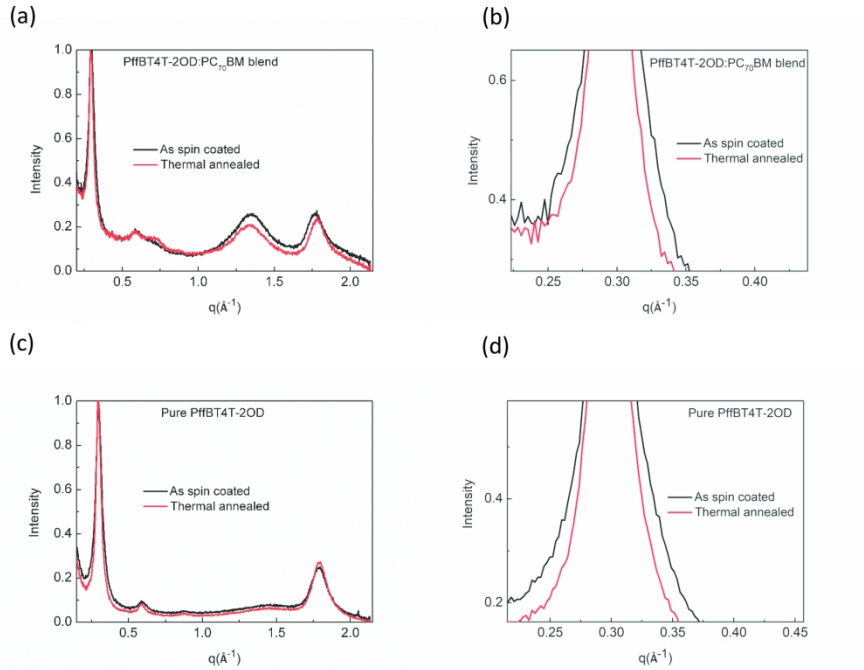

Figure 2

254x190mm (300 x 300 DPI)

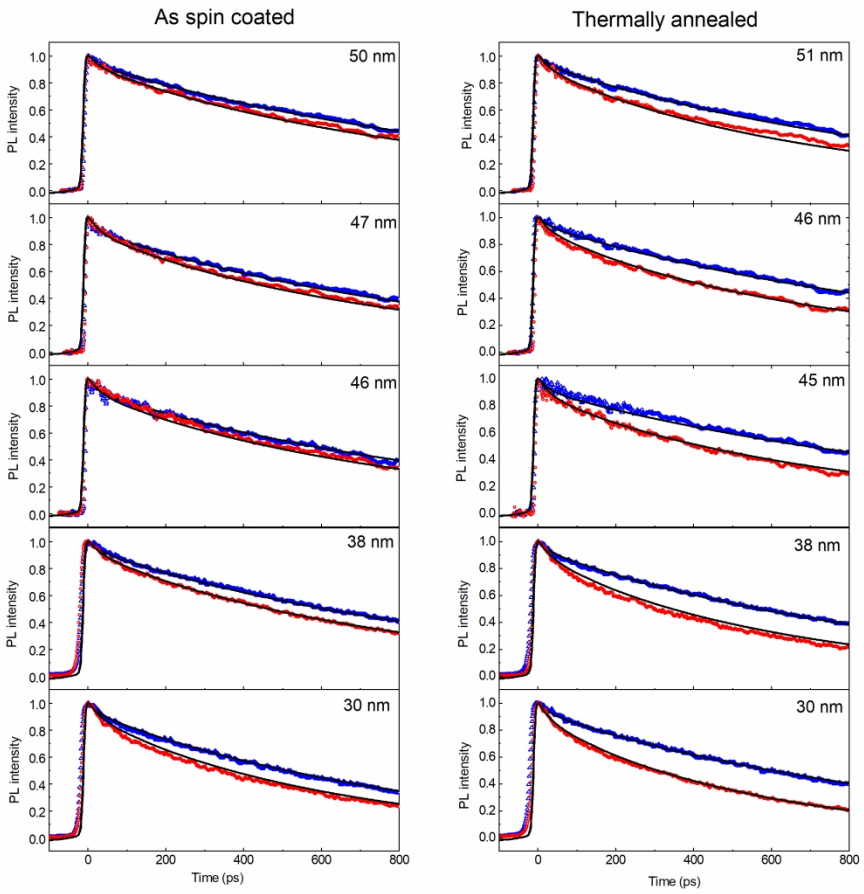

Figure 3

269x271mm (300 x 300 DPI)

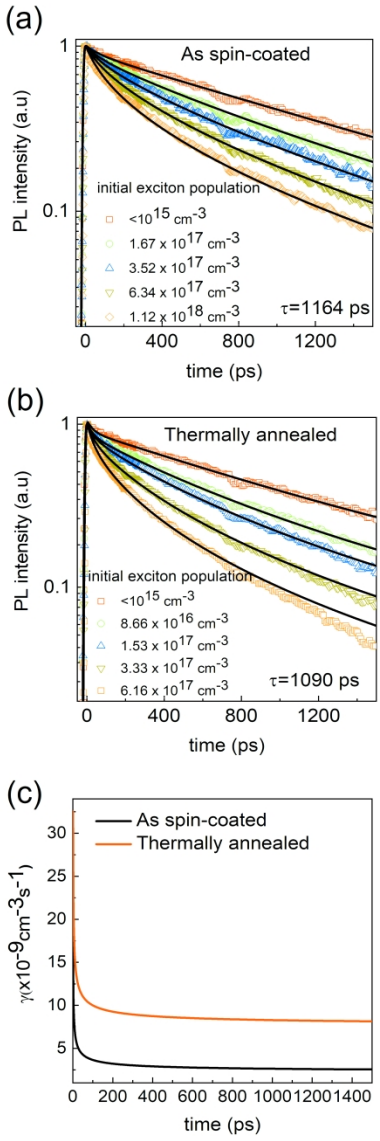

Figure 4

228x571mm (300 x 300 DPI)

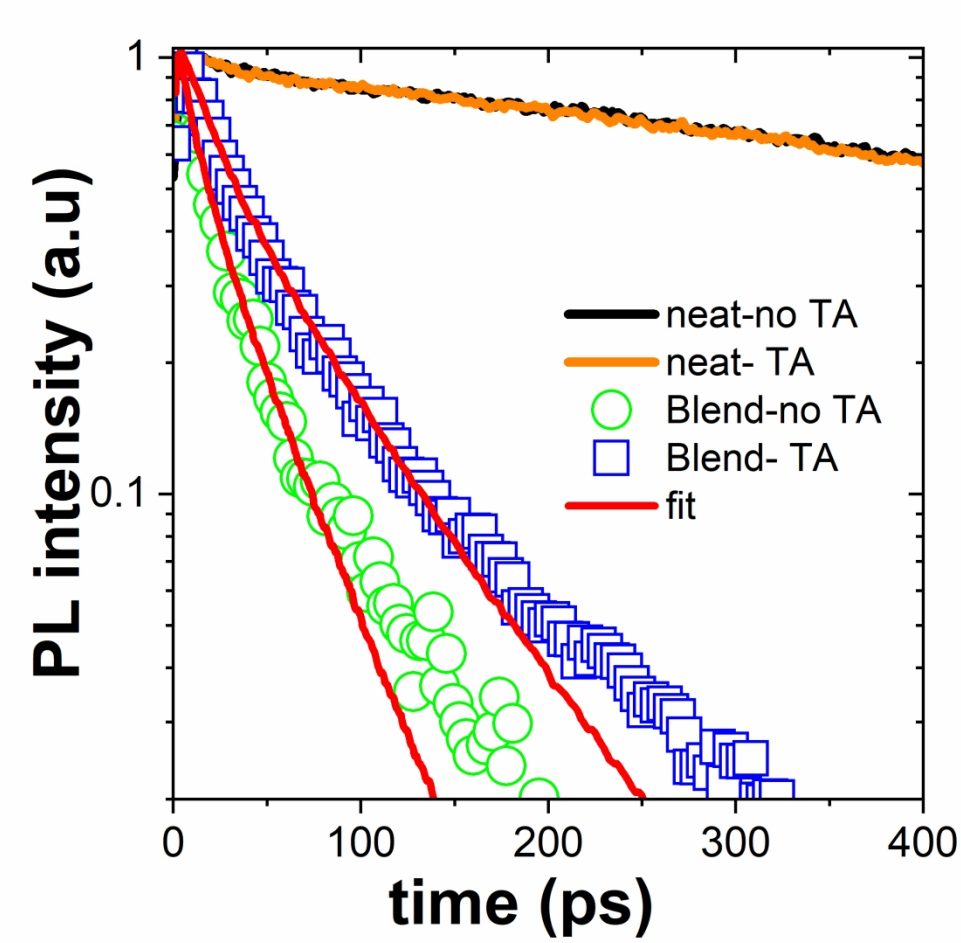

Figure 5

199x189mm (300 x 300 DPI)

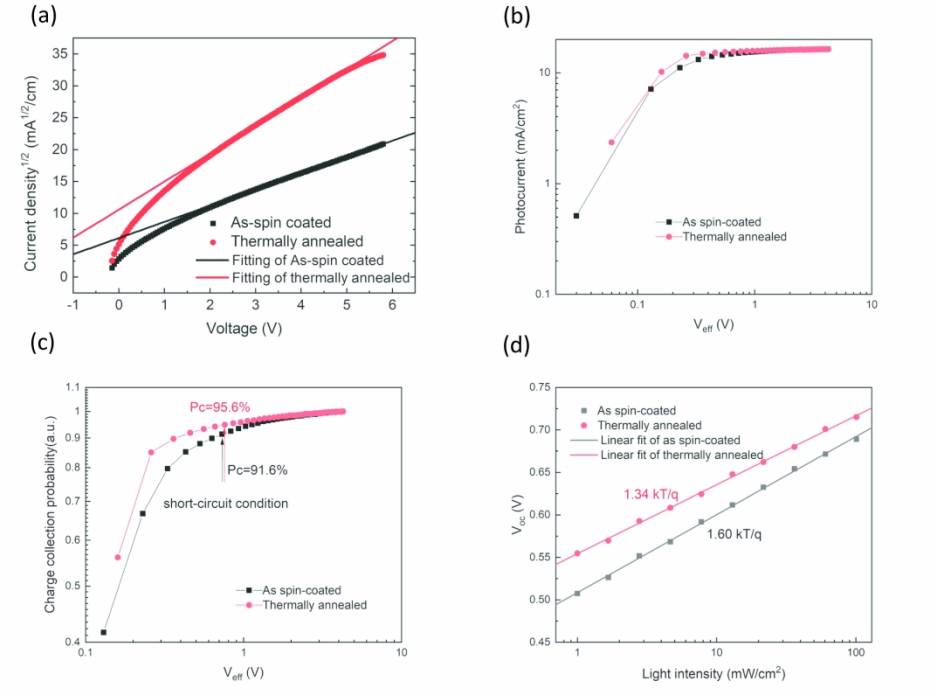

Figure 6

254x190mm (300 x 300 DPI)